Unseasonal atmospheric river drives anomalous glacier accumulation in the ablation season of the subtropical Andes

Claudio Bravo[1], Sebastián Cisternas[1], Maximiliano Viale[2], Pablo Paredes[1], Deniz Bozkurt[3,4,5], Nicolás García-Lee[1,6]

5

[1]Centro de Estudios Científicos, Valdivia, Chile.
[2]Instituto Argentino de Nivología, Glaciología y Ciencias Ambientales, Mendoza, Argentina.
[3]Departamento de Meteorología, Universidad de Valparaíso, Valparaíso, Chile.
[4]Centro de Ciencia del Clima y Resiliencia, Santiago, Chile.
10 [5]Center for Oceanographic Research COPAS COASTAL, Universidad de Concepción, Concepción, Chile
[6]MSc. Program in Water Resources, Universidad Austral de Chile, Valdivia, Chile.

Correspondence to: Claudio Bravo (cbravo@cecs.cl)

Abstract. Climate change is associated with changes in the frequency and intensity of extreme weather events. These changes are impacting the mass balance of Andean glaciers, a phenomenon that requires further detailed investigation. Among these

15 events, atmospheric rivers (ARs) play a significant role in influencing glacier mass balance, potentially leading to either accumulation or melting events. To assess the impact of ARs on Andean glaciers, we analysed an unseasonal event that occurred at the end of January 2021, marked by extreme rainfall, landslides, and flash floods in the lowlands, during the typically dry summer period. Satellite imagery and meteorological observations in the glaciated Maipo River basin and its Olivares River sub-basin (33°S) enabled the characterisation of this event and its basin-scale impacts. Moreover, a glacier

20 mass balance model allows us to quantify the effects on the Olivares Alfa Glacier (4284 to 4988 m a.s.l.) over the context of the preceding six hydrological years. The significant water vapour transport by the AR led to substantial snow accumulation on the Maipo River glaciers, confirmed by the post-event snowline observed at 2463 m a.s.l. In the Olivares River sub-basin, the 0°C isotherm dropped during the event to an elevation of 3250 m a.s.l., below the frontal zone of all glaciers in this sub-basin. The mass balance model for the Olivares Alfa Glacier during the dry 2020/21 hydrological year showed a trend toward

25 negative values at the beginning of the ablation season, aligning with previous years and the prevailing mega-drought conditions. However, the AR event offset this trend, bringing the mass balance closer to equilibrium. This demonstrates that an unseasonal accumulation event can significantly counteract the broader seasonal trends affecting subtropical Andean glaciers. Our study sheds light on the impacts of extreme and unseasonal snow accumulation events on glacier mass balance in the high Andes, particularly those associated with ARs, a synoptic feature projected to become more common in a warming

30 climate.

1 Introduction

Glaciers, with their high sensitivity to climatic variations, stand as crucial indicators of climate change in regions spanning from tropical to polar areas. Central to their behaviour is the mass balance, a critical metric capturing the net gain or loss of ice and snow over specific periods. The mass balance, in turn, is profoundly influenced by the prevailing atmospheric

35   conditions during specific periods, such as the hydrological year. Long-term observations in the Andes have shown a marked tendency to glacier mass loss, largely attributed to increases in air temperature and/or decreases in precipitation (Braun et al., 2019; Dussaillant et al., 2019). However, embedded in this overall negative mass balance trend, there are typically large interannual variability in atmospheric conditions, and so in the annual mass balance of glaciers. In the subtropical Andes, the atmospheric interannual variability is mainly modulated by global-scale atmospheric-oceanic circulation patterns such as El

40   Niño Southern Oscillation (ENSO), Southern Annular Mode (SAM), and the Interdecadal Pacific Oscillation (IPO), among others (Garreaud et al., 2009). For instance, the warm ENSO phases (El Niño) are usually associated with positive anomalies in snowfall in the subtropical Andes of Chile and Argentina, while cold ENSO phases (La Niña) sometimes result in below-average snow accumulation (Masiokas et al., 2020). Besides global-scale phenomena modulating annual mass balance, individual extreme synoptic-scale events, such as intense heat waves or precipitation events, can strongly modulate annual

45   mass changes of Andean glaciers. To our knowledge, the impact of individual extreme events on the annual mass balance of Andean glaciers has not been assessed yet, despite their increasing significance with climate change (Poveda et al., 2020).

While significant advances have been made in understanding extreme temperature and precipitation events in the subtropical Andes and their associated synoptic conditions (Bozkurt et al. 2016; Viale et al., 2018; Feron et al., 2019; Jacques-Coper et al., 2016 and 2021; Demortier et al., 2021; Valenzuela et al. 2022; Gonzalez-Reyes et al., 2023; Garreaud et al., 2024), their

50   role on glaciers mass balance remains largely unexplored. One pertinent subject of inquiry relates to the occurrence of atmospheric rivers (ARs) leading to intense precipitation events in the subtropical Andes (Viale et al., 2018). ARs are narrow, elongated corridors of intense water vapour transport, often situated ahead of ocean cold fronts which primarily make landfall and discharge its vapour as precipitation on the western coasts of the mid-latitude continents (Guan and Waliser, 2019). Notably, the most intense ARs typically lead to extremely heavy orographic precipitation on mountainous western coasts, and

55   so to severe hydrometeorological hazards (Ralph et al., 2006; Leung and Qian, 2009; Neiman et al., 2011; Payne et al., 2020). In the semi-arid subtropical Andes, ARs constitute the main source of water, particularly during the winter season (Viale et al., 2018; Saavedra et al., 2020). Indeed, Saavedra et al. (2020) quantified that AR events account for 50% of the total annual snow accumulation, favoured by 2.5 times more intense snowfall events than non-AR snowfall events. However, their effects on glaciers can be opposed, as they can bring both significant snowfall accumulation and extreme ice/snow melting at mid-

60   latitudes glaciers (Guan et al. 2010; Little et al., 2019; Kropač et al., 2021). For instance, Little et al. (2019) showed that at Brewster Glacier in New Zealand's Southern Alps, the most intense ablation and accumulation days coincide with ARs that transport exceptionally high levels of water vapour, depending on their associated thermal conditions. This dual role of ARs in driving high accumulation and melting events is not limited to mid-latitudes. In polar latitudes, such as Antarctica and

Greenland, ARs events also exert a two-fold influence. These events can contribute to increased snowfall accumulation on the

65   vast ice sheets, potentially mitigating its mass loss (Mattingly et al., 2018; Wille et al., 2021; Adusumilli et al., 2021; Maclennan et al., 2022). Conversely, they have been implicated in driving episodes of extreme warm temperatures, intense surface melting and liquid precipitation events in West Antarctica, the Antarctic Peninsula, and Greenland, particularly along the coastal zones, causing concerns about ice sheet stability (Wille et al., 2019, 2022; Xu et al., 2021; Box et al., 2022; Mattingly et al., 2023).

70   The role of ARs in shaping glacier dynamics is complex and contingent upon multiple factors including synoptic conditions, seasonal time occurrences of the AR events, and the altitudinal and latitudinal location of the glaciers. As we introduced before, these multiple influential factors can lead to divergent outcomes in glacier response. For instance, when favourable conditions exist such as glaciers located over the 0°C isotherm, ARs can trigger substantial snow accumulation events. Conversely, ARs can lead to glacier and snow melting events through several mechanisms, including large-scale sensible heat transport (e.g.,

75   Bozkurt et al., 2022; Wille et al., 2022), rain-on-snow events, and an increase in cloud cover and downward longwave radiation over mountains (Chen et al., 2019; Zou et al., 2021; Wille et al., 2022). Furthermore, ARs can initiate post-event feedback mechanisms on glacier surfaces, for example, notably contributing to glacier albedo changes (e.g., Box et al., 2022). All these factors and their combination are important to be analysed and quantified.

Beyond the scientific realm, understanding the impact and role of ARs in the Andean cryosphere holds profound societal

80   significance. In the semi-arid Andes, glaciers constitute natural water reservoirs, storing vast amounts of freshwater as ice, which gradually feeds rivers, supplying water for agriculture, drinking, and hydropower generation for over 10 million people (Ayala et al., 2020; Crespo et al. 2020). Therefore, ARs can influence annual glacier dynamics, impacting the timing and magnitude of freshwater release for managing this vital resource. Furthermore, ARs can lead to extreme events such as floods and landslides triggered by rain-on-snow events (e.g., Guan et al., 2016; Dolant et al., 2017; Somos-Valenzuela et al., 2020;

85   Rutllant et al., 2023), with devastating consequences for communities, infrastructure, and economies. Assessing these AR impacts contributes to a deeper understanding of glacier hazards triggered by extreme weather events (e.g., Carey et al., 2012) and enhances the long-term sustainability and resilience of regions reliant on glacier meltwater in the central Andes.

In this work, our objective is to evaluate the role of an extraordinary dry-season precipitation event, triggered by an AR, over the glaciers of the Maipo River basin, especially over the Olivares Alfa Glacier located in the Andes at 33°S (Fig.1). This

90   unseasonal precipitation event occurred between 28 and 31 January 2021, and characterized by heavy rainfall, hail, and lightning in the lowlands, and heavy snowfall in the high mountain. First, we assess whether accumulation or melting during this event predominantly influences the annual mass balance. Secondly, we analyse the drivers behind the glacier mass balance response to the AR event by quantifying the surface energy balance. Thirdly, we quantify how a single extreme unseasonal precipitation event can alter the mass balance trend for this particular year and in the context of seven hydrological years.

95   Finally, we analyse the potential feedback mechanisms related to this event and discuss its implications, particularly in the context of the well-known large-scale glacier mass balance forcing as ENSO. To accomplish these research objectives, we use remote sensing, radiosonde data, and available meteorological observations located in the glaciarised high Olivares River sub-

basin. These meteorological data were also used as input for the COSIPY v1.3 mass balance model (Sauter et al., 2020), which
allowed us to quantify the impact of this AR-related precipitation on the annual mass balance of the Olivares Alfa Glacier. To

100 our knowledge, this study represents the first comprehensive examination of AR impacts on glacier mass balance in the Andean
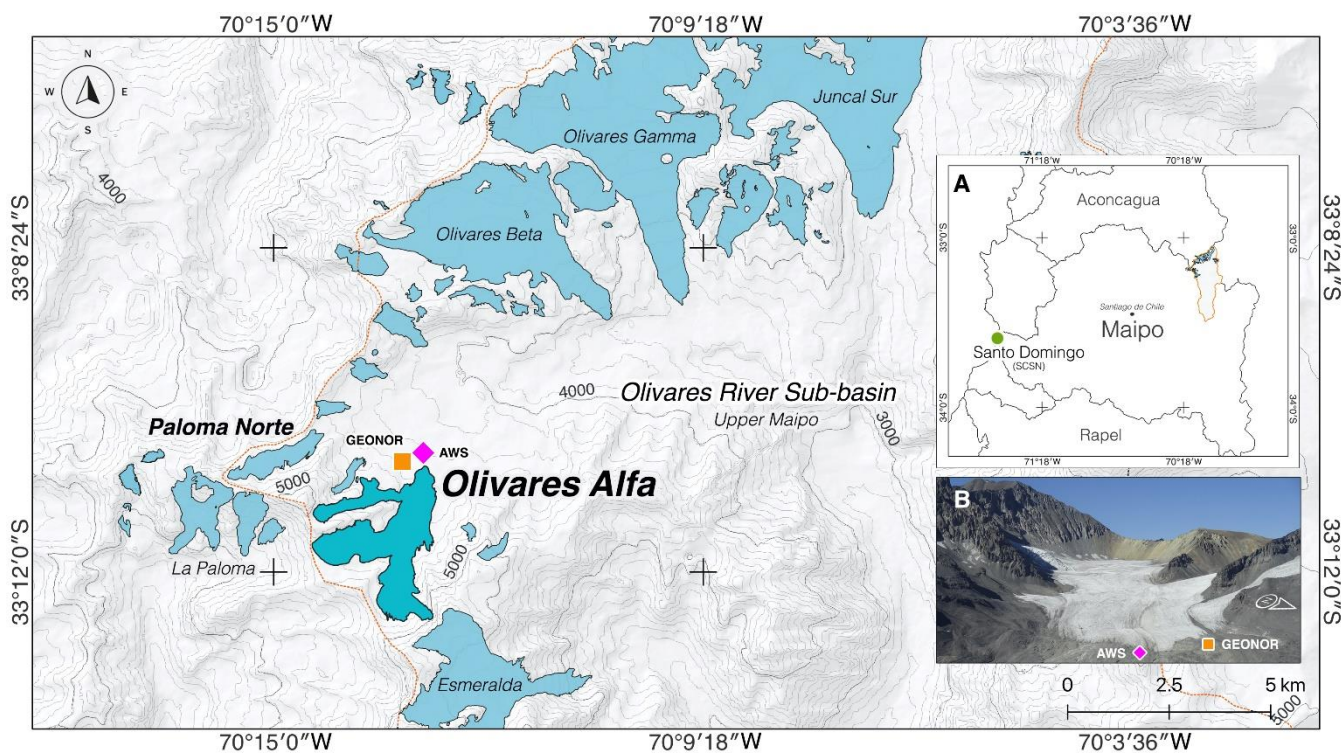region.

Figure 1. Glaciers of the Olivares River sub-basin and the location of the Automatic Weather Station (AWS, magenta colour) and
105 **pluviometre (GEONOR, orange colour) close to Olivares Alfa Glacier. Inset A is the regional context of the Maipo River basin (black**
line) and the Olivares River sub-basin (orange line). Santo Domingo corresponds to the place from which radiosondes are launched.
Inset B, is a photograph taken on 5 February 2015 by the author with a detailed view of the Olivares Alfa Glacier. Magenta and
orange symbols indicate the AWS and the GEONOR localisation, respectively.

2 Study area and the Atmospheric River event

110 We conducted our assessment at two different river basin scales: first at the Maipo River basin and then at the Olivares River
sub-basin of the Maipo River (Fig. 1). The Maipo River basin is responsible for supplying 70% of the water consumed in
Santiago de Chile city (Fig. 1a, Ayala et al., 2020), and contains around 1000 ice bodies comprising a total glacier area of 388
km^2 (Barcaza et al., 2017). Our analyses focused on the Olivares River sub-basin, which hosts a glaciarised area of
approximately 70 km^2 centred around 33°10' S 70°10'W. Within the Olivares River sub-basin lies the highest glaciers in the

115 Maipo River basin, ranging from 3500 to 5800 m a.s.l. (Ayala et al., 2020), whose ice masses have experienced the most

significant rate of ice loss compared to glaciers in other Maipo River sub-basins between 2000 and 2013 (Farías-Barahona et al., 2020).

The Olivares River sub-basin is home to several glaciers, including Olivares Alfa, Olivares Beta, Olivares Gamma, and Juncal Sur (Fig. 1). These glaciers exhibit clear signs of thinning and retreat (Farias-Barahona et al., 2020; Malmros et al., 2016).

120 Additionally, they have shown a trend towards darkening their surfaces since the 1980s (Shaw et al., 2021; Barandun et al., 2022). Finally, glacier simulations, detailed in the next section, focused on the Olivares Alfa Glacier (Fig.1), a mountain glacier with two accumulation zones, both primarily oriented towards the northeast and with a mean elevation of 4574 m a.s.l. According to Shaw et al. (2021), the estimated area of this glacier as of March 2020 is 3.2 km^2. Historical satellite images reveal that the Olivares Alfa was formerly part of a continuous glacier that extended over most of the western headwater of

125 the sub-basin. Malmros et al. (2016) quantified a significant glacier area loss of 63% between 1955 and 2013, indicating a gradual fragmentation of the ice mass over the years.

In late January 2021, the subtropical Andes of Chile and Argentina experienced a major and unusual precipitation event produced by an unseasonal and zonal-oriented AR (Fig. 2a). Precipitation and ARs are almost absent in summertime (dry season) over the western slopes of the subtropical Andes and the central Chilean lowlands (Viale and Garreaud, 2014).

130 According to the ERA5 reanalysis data (Hersbach et al 2023), the AR was classified as category 1 on the coastal grid points between 34.5°S and 39°S (Figs. 2b-c), in the five-category scale proposed by Ralph et al. (2019). AR category 1 around 35°S in summertime occurs roughly three times every 10 years, and higher categories have even lower frequencies. The actual AR event unleashed an unprecedented, record-breaking accumulation of precipitation over the course of four days between January 28 and January 31, with totals over 100 mm across central-south Chile (Fig. 2c, and Valenzuela et al., 2022). The storm's first

135 phase (28–29 January) occurred in a warm, summertime environment; while during the second phase (30–31 January), the AR quickly dissipated, leaving residual moisture and forming a cut-off low, that fuel intense convection, rain, lightning, and hail, leading to significant societal disruptions and economic losses (Valenzuela et al., 2022).

This extraordinary event bore several distinctive hallmarks, making the storm even strong for winter storms. Such climatic anomalies are a rarity, with historical records documenting similar storms occurring only 2–3 times in the past century

140 (Valenzuela et al., 2022). This AR-related precipitation event serves as the focal point of our study, as we assess its influence on the annual Olivares Alfa glacier's mass balance, marking the first AR-glacier impact study of its kind in this region.
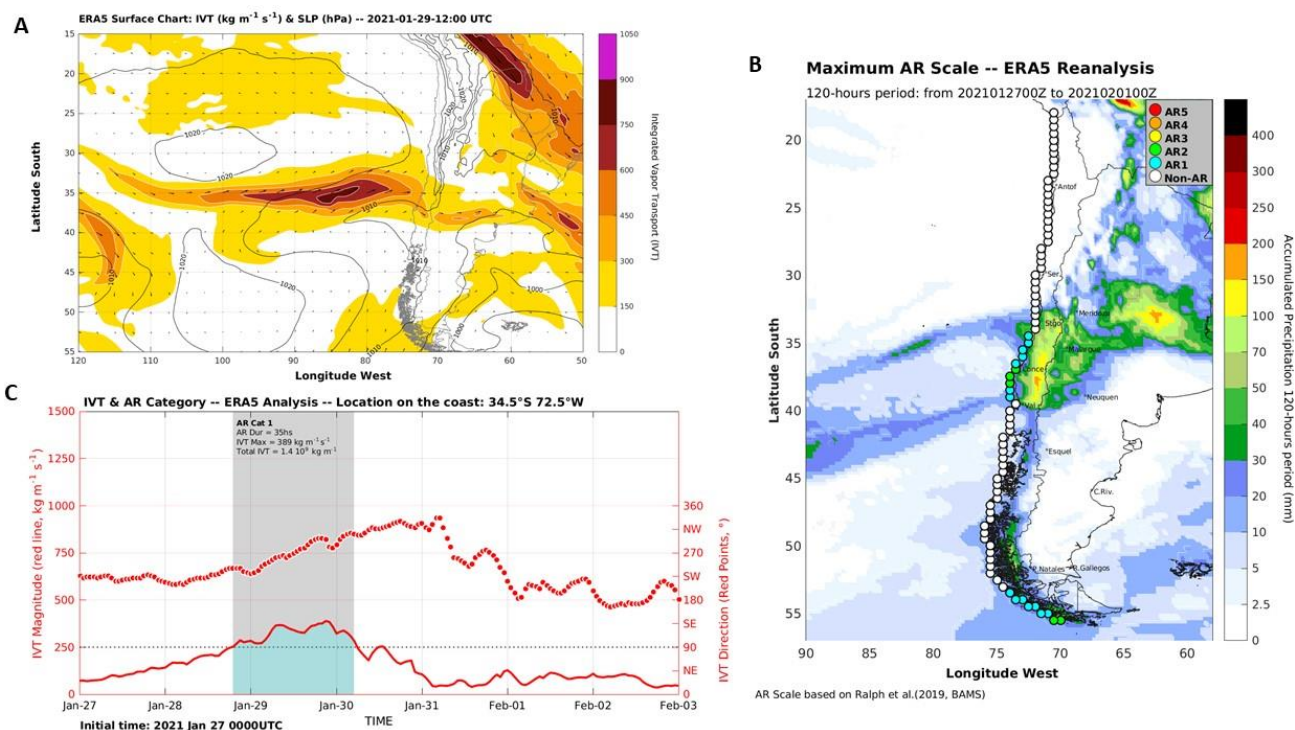
Figure 2. Reanalysis ERA5 showing the unseasonal atmospheric river that made landfall in central Chile. a) Surface chart with the
145 **Sea Level Pressure (SLP, lines in hPa) and the Integrated Vertical Transport (IVT, shaded in kg m^{-1}s^{-1}) at 1200UTC on 29 January 2021. b) Storm total precipitation accumulated from 0000 UTC on 27 January to 0000 UTC on 01 February 2021 (shaded in mm). The color-coded circles on the Pacific coast show the AR category in the Ralph's scale (Ralph et al. 2019) reached by the current AR. c) Time series of IVT magnitude and direction on the coastal grid point at 34.5°S, showing the AR conditions.**

3 Materials and methods

150 In our approach to address the research questions, we employ a two-scale analysis: the basin and glacier scales analyses.

3.1 Basin-scale analysis

Firstly, at the Maipo River basin scale (Fig. 1a), we aim to estimate if glaciers were subject to accumulation and/or melting. We utilised the MODIS daily snow cover product (Terra MOD10A1 and Aqua MYD10A1, V0006, 500 m resolution) (Hall et al., 2006) to derive the snowline elevation in the Maipo River basin. The snowline elevation was calculated using the method 155 developed by Krajčí et al. (2014) over the period from April 2001 to March 2021. This approach enables us to assess the exceptional nature of the AR event at a regional scale and in the context of the past 20 years.

Secondly, we estimated the elevation of the 0°C isotherm or freezing level to assess the glacier area experiencing melting by using radiosonde and in-situ data. The radiosonde data registered by the Santo Domingo station (33.63°S, 71.65°W, Fig. 1a) was obtained from the NOAA Integrated Global Radiosonde Archive (IGRA) database. Furthermore, we utilised air

160 temperature data from an Automatic Weather Station near the front of the Olivares Alfa Glacier (AWSOA, 4220 m a.s.l., 33°10' S, 70°13' W, Fig. 1-1b), as well as multiple air temperature sensors located at different elevations in the Olivares River sub-basin (3606, 4004, 4459, 4466 and 4771 m a.s.l.). The freezing level was estimated using linear regression of the hourly air temperature records at the different elevations. To ensure accuracy and reliability, we compared the 0°C isotherm estimated from the Santo Domingo radiosonde data with the one derived from the air temperature sensors in the sub-basin.

165 The estimated snowline elevation and freezing level enable us to estimate the glacier area experiencing melt and/or accumulation before, during, and after the precipitation event in the Maipo River basin and the Olivares River sub-basin. The estimated snowline and freezing level were then compared with the hypsometry of the basin's glaciers, derived from glacier outlines from the year 2021 and the AWW3D30 digital elevation model (DEM).

3.2 Glacier-scale analysis

170 To assess the impact of the precipitation event on the glacier mass balance, we utilised the coupled snowpack and ice surface energy and mass balance model "COSIPY" (v1.3), developed by Sauter et al. (2020). This model employs state-of-the-art equations and parameterizations to estimate turbulent fluxes. Input data for the model were collected from two sources near the Olivares Alfa Glacier: the AWSOA and the precipitation sensor GEONOR T200B-M (see Table 1 for sensor details and Figure 1 for location). These observations include air temperature, air relative humidity, wind speed, atmospheric pressure,

175 precipitation, shortwave and longwave radiation (Table 1, Fig. 3). Direct longwave radiation measurements were only available from September 2016 onwards. Therefore, data derived from ERA5 reanalysis were utilised after undergoing bias correction with the aid of direct observations (Lopes et al. 2022; Fig. 3g) to cover the complete period from April 2014 to March 2021. Consequently, we simulated the total mass balance of seven hydrological years.

Furthermore, glacier delimitations were obtained from medium and high-resolution imagery for the modelling period of 2013

180 to 2021, along with the AW3D30 DEM data from the Japan Aerospace Exploration Agency. The model distributes the meteorological variables over the glacier surface at a spatial resolution of 100 m.

Due to the scarcity of detailed and consistent snow-depth observations on the glacier surface at the beginning of each hydrological year (i.e., April in the subtropical Andes), we adopted an annual approach when running the model. This entailed initialising the model with a no-snow starting condition for each year of the period of interest.

185 Analysed outputs of the model include total mass balance (in m w.e.) and surface energy fluxes, such as turbulent fluxes and net short and longwave radiation (in W m^{-2}). These model outputs were analysed to assess the impact of the event on the energy balance and on the glacier's annual mass balance. In addition, a comparison of the annual mass balance series was made with previous hydrological years. Total mass balance was assessed rather than surface mass balance, to incorporate feedback and changes in internal mass balance, melt and refreezing processes (Sauter et al., 2020). To further evaluate the impact of this

190 unseasonal precipitation event, we also simulated the 2020/21 hydrological year's mass balance under a hypothetical scenario without the AR's influence, removing the accumulation attributed to the summer-2021 AR and detrending the mass balance time series post-event. The behaviour from previous similar years (i.e. those years with negative mass balance until the end of

January) was derived and applied to the detrended 2020/21 accumulated mass balance time series. We follow this approach to
discard mass balance feedback post-AR event, for instance, related to the increase in the albedo which reduces the incoming
195   shortwave radiation.

Table 1. Sensors of the Automatic Weather Station located near the front of Olivares Alfa Glacier (AWSOA), at 33°10' S, 70°13' W, 4220 m a.s.l.

| Variable	Units	Instrument Type	Manufacturer	Model	Accuracy
Air temperature (AirT)	°C	Temperature and relative humidity probe	Vaisala	HMP 155	±0.2 °C
Relative humidity (RH)	%	Temperature and relative humidity probe	Vaisala	HMP 155	±2%
Wind speed (WS)	m s^{-1}	Wind monitor	R. M. Young	Heavy Duty Wind Monitor-HD-Alpine 05108-45	± 0.3 m/s or 1% of reading
Wind direction (WD)	degrees	Wind monitor	R. M. Young	Heavy Duty Wind Monitor-HD-Alpine 05108-45	± 3 degrees
Precipitation (PP)	mm	Precipitation - rain gauge	Geonor	T200B-M	±0.1%
Incoming Shortwave Radiation (SWR)	W m^{-2}	Pyranometer	Kipp and Zonen	CMP3	±10%
Incoming Longwave Radiation (LWR)	W m^{-2}	Pyrgeometer	Kipp and Zonen	CGR3	±10%
Atmospheric pressure (AP)	hPa	Barometer	Vaisala	PTB-110	±0.3 hPa at +20 °C

200
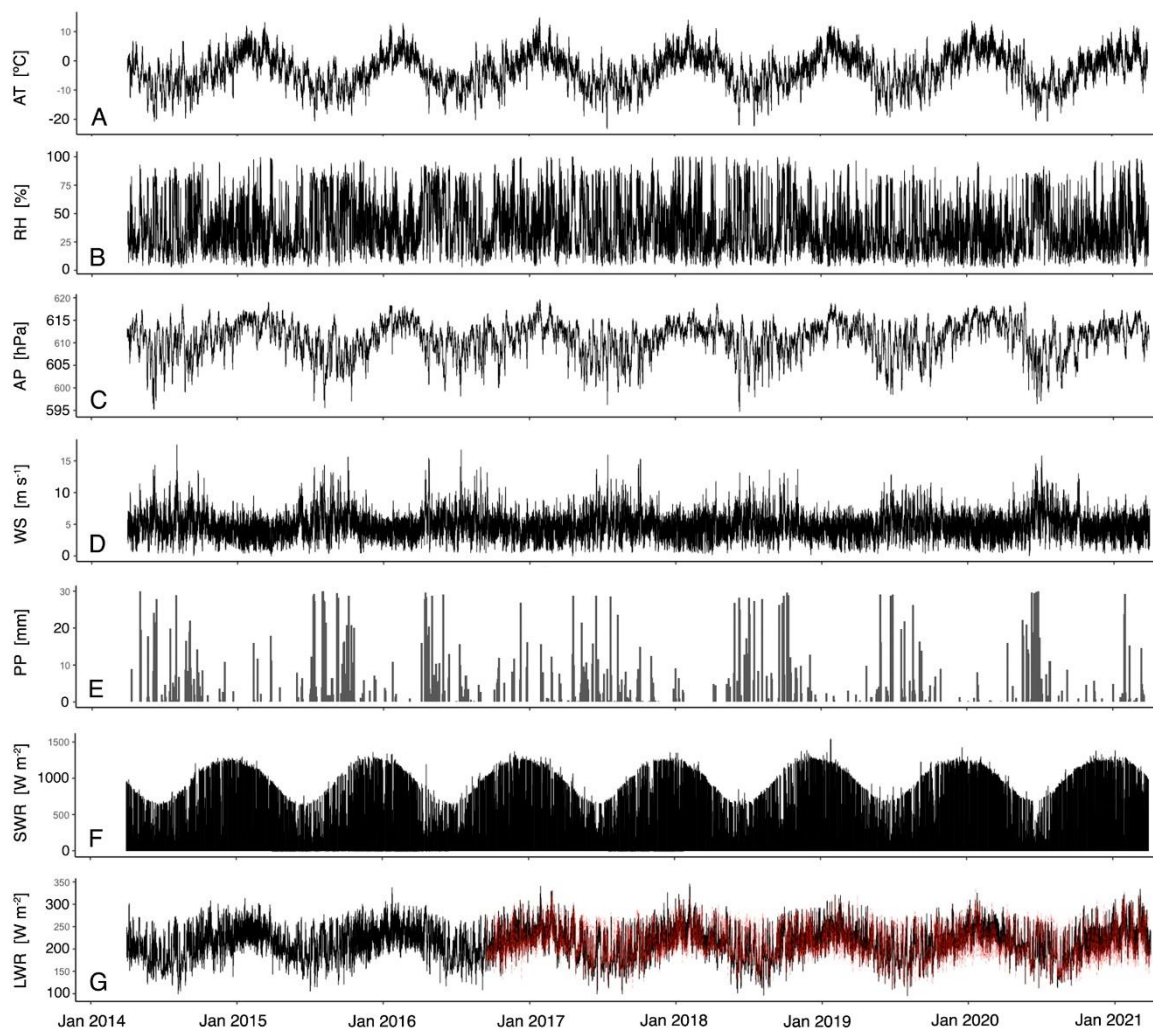
Figure 3. Hourly time series of the meteorological variables observed at the AWSOA and the GEONOR T200B-M during the period April 2014 to March 2021. a) Air temperature, b) relative humidity, c) atmospheric pressure, d) wind speed, e) total precipitation, f) incoming shortwave radiation and g) incoming longwave radiation. Red in g) corresponds to observations at AWSOA and black corresponds to the bias-corrected time series using ERA5.

3.3 Atmospheric River events 2014-2021

Furthermore, to put in historical context the impact of the summer-2021 AR, we evaluate the impact of past ARs on the simulated glacier mass balance in each hydrological year. We search for the AR conditions on the Pacific coastal grid points of the reanalysis ERA5 in central Chile (30°S-35°S) over the 2014-2021 period (7 years). AR conditions are ranked into five categories according to Ralph et al. (2019) scale; category 1 being the lowest and category 5 being the highest. The scale combines the maximum moisture transport integrated into the vertical column of the atmosphere, i.e., the Integrated Vapour

9

Transport (IVT), with the duration of the AR conditions, determined by the time when IVT is always greater than 250 kg m^{-1} s^{-1}. AR category 1 is primarily associated with beneficial precipitation-related impacts, while AR category 3 can be a balance

215   between beneficial and hazardous and AR category 5 is primarily hazardous. For further details on the AR scale see Ralph et al (2019). In our study, we retain AR events when at least AR category 1 occurred in one of the coastal grid points between 30° and 35°S. AR events in central Chile typically have more than one grid point with AR category >= 1 affecting this latitude range, and so the onset and demise of the AR events are established by the initial and final time of the overlapping period with AR conditions between all considered coastal grid points. For further analyses, we retained two variables as measures of AR

220   event intensity: the maximum AR category and the maximum IVT instantaneous value among all grid points with AR conditions. The AR catalogue used here is shown in Table S1.

4 Results

### 4.1 Snowline elevation in the Maipo River basin

In the Maipo River basin, the snowline elevation from MODIS data was estimated to be around 4700 m a.s.l. before the

225   summer-2021 AR event. This elevation is over 75th percentile of the distribution of the snowline for the January and February months between 2001 and 2021, where the snowline typically ranges between 3900 and 4500 m a.s.l., with higher glaciers sections being snow-covered at this summertime. During the event, the snowline elevation sharply decreased, reaching a minimum elevation of 2463 m a.s.l., which is lower than the 0°C isotherm's minimum (~3250 m a.s.l., next section). Immediately post-event measurements placed it among the lowest January and February snowline elevations observed from

230   MODIS SNOW for the period 2001 to 2021. The average summer snowline elevation for this period is 4250 m a.s.l. After the event, the snowline elevation gradually increased reaching an elevation like January 2021, but did not return to its pre-event elevation by the end of the hydrological year.
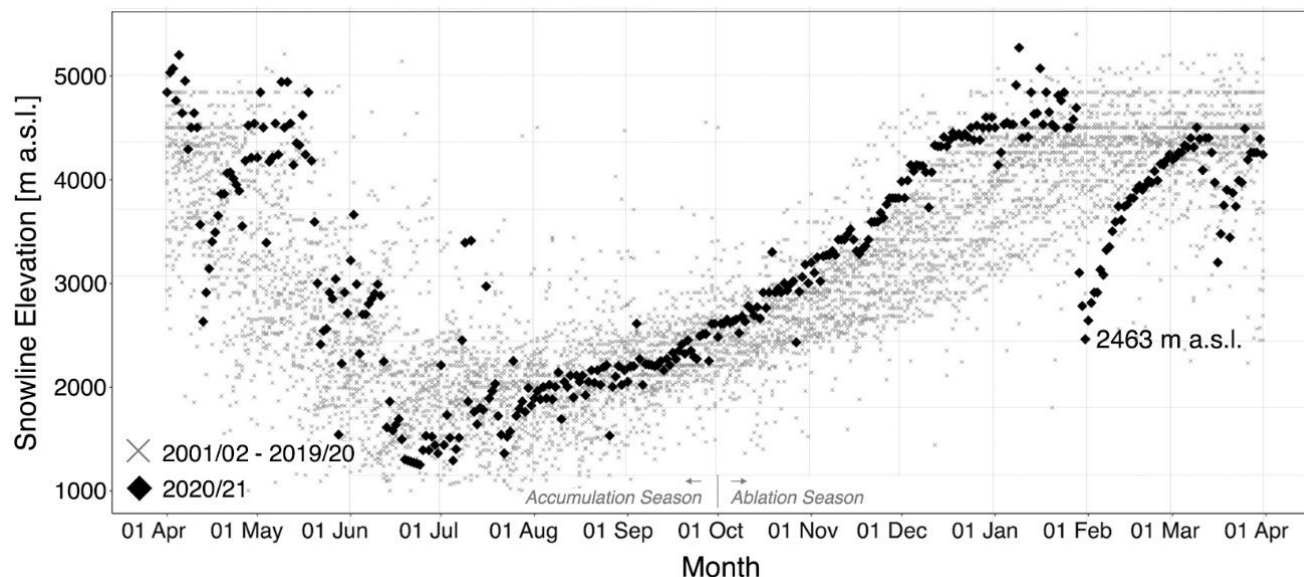
Figure 4. Snowline time series at the Maipo River basin for the hydrological years between 2001 and 2019 (grey crosses) and 2020-2021 (black diamonds).

4.2 0°C isotherm elevation at the Olivares River sub-basin

On the days before the event (25 to 28 of January), 0° isotherm elevation was estimated to be between 4000 and 4500 m a.s.l. with a marked daily cycle (Fig. 5). The 0°C isotherm estimations from the in-situ air temperature sensors and radiosonde data were practically the same. At the onset of the event (i.e., 29 January), the 0° isotherm decreased to around 3700-3900 m a.s.l., and the next day, it further decreased to 3250 m a.s.l. This last value corresponds to the minimum 0°C isotherm during the event and coincides with the maximum precipitation rate recorded by the GEONOR sensor (Fig. 5). Around this minimum 0° isotherm time, all glacier areas in the Olivares River sub-basin were accumulating snow during the first half of the 30 January. A rapid increases of the 0° isotherm elevation occurred after mid-day of 30 January, resulting in positive temperatures in the lower elevation glacier areas, particularly in the frontal sections of the Olivares Gama and Juncal Sur glaciers, which extend up to around 3800 m a.s.l. On 31 January, the 0° isotherm decreased to similar values of the previous day, oscillating between 3300-3500 m a.s.l., coinciding with the event's second-highest precipitation rate. Consequently, the total glacier area of the basin experienced negative air temperatures. On the days after 1 February, no precipitation was recorded, and the 0° isotherm oscillated between 3500 to 3800 m a.s.l., until 3 February when it quickly rose to pre-event levels. During the post-event days (after 1 February), a discrepancy was observed between the 0° isotherm measurements from in-situ temperature sensors and radiosonde data.

11
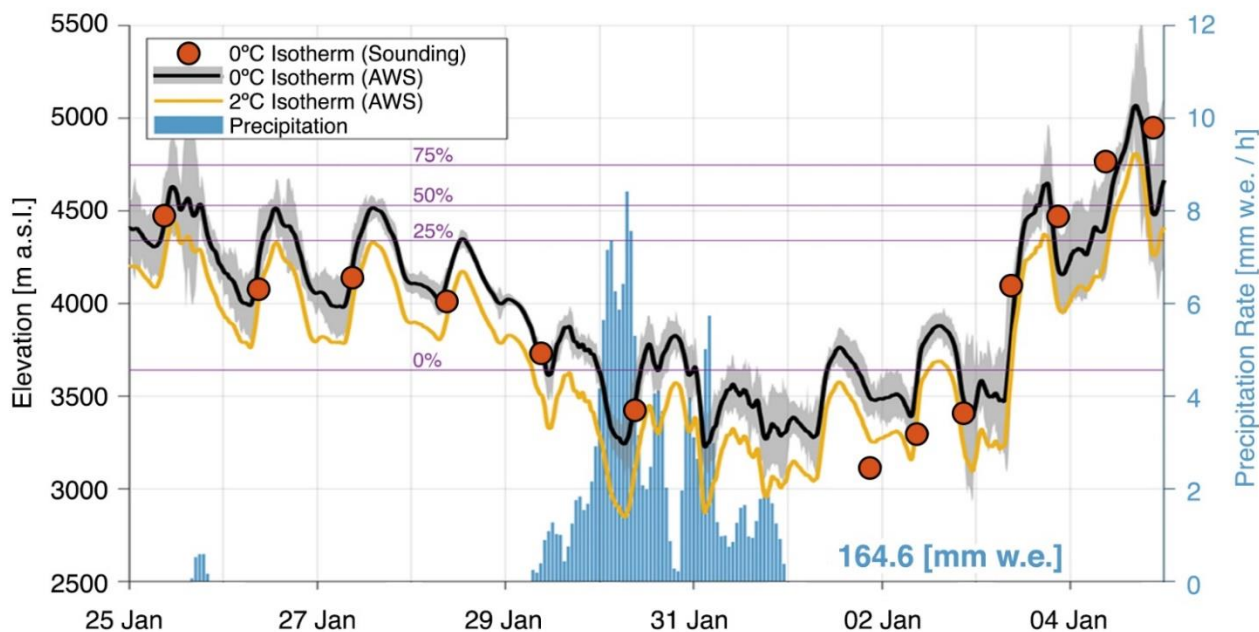
Figure 5. Time series of the 0°C isotherm. The black line corresponds to the calculated values using AWSOA and AWS DGA. Red circles correspond to the 0°C isotherm obtained from the Santo Domingo radio sounding. Bars are the hourly precipitation recorded
255 **by the GEONOR T200B-M. Percentages corresponding to the glacier area hypsometry of the Olivares River sub-basin. As a reference 2°C isotherm is also shown with a yellow line.**

4.3 Surface fluxes energy changes during the event at the Olivares Alfa Glacier surface

Summertime (DJF) averaged fluxes from 2014 to 2021 shown in Table 2 indicate the main source of energy on the glacier surface is the net shortwave radiation (mean of 120 W m^{-2}), and the main energy loss is from the net longwave radiation (-53

260 W m^{-2}). Latent heat flux, predominantly negative (mean of -39 W m^{-2}), indicates that the glacier surface is melting during the ablation season. Conversely, sensible heat flux is positive (mean of 18 W m^{-2}), reflecting a lower glacier surface temperature compared to their surrounding air temperature. Ground heat fluxes vary between positive and negative values during nigh time and daytime, respectively (Fig. 6). The available melt energy typically reaches a mean value of 54 W m^{-2}, with the maximum around 150 W m^{-2}, as estimated just before the AR event (Fig. 6).

265 During the summer-2021 AR event, these typical summertime values changed (Fig. 6). There was a notable decrease in both the net shortwave and longwave radiation on the 29 and 30 January, coinciding with the maximum precipitation rate and AR moisture transport (Figs. 2b and 5). The event's mean net shortwave and longwave radiation values during the event were 22 and -17 W m^{-2}, respectively. Continuous cloud cover during the storm reduced the variability in net longwave radiation, which turned positive for a short period. Turbulent fluxes tended to decrease as well. Latent heat flux dropped (i.e. became less

270 negative) due to added atmospheric water vapour by the AR and the decrease of the melting rate in the glacier surface, diminishing the humidity gradient between the surface and air. Similarly, sensible heat flux decreased because of the reduced

air temperature during the storm and the persistent cloud cover, lessening the temperature gradient between the surface and air. During the 30 and 31 January, negative values of sensible heat fluxes were estimated, indicating that the glacier surface was warmer than the surrounding air. Melt energy was again available three days after the event.
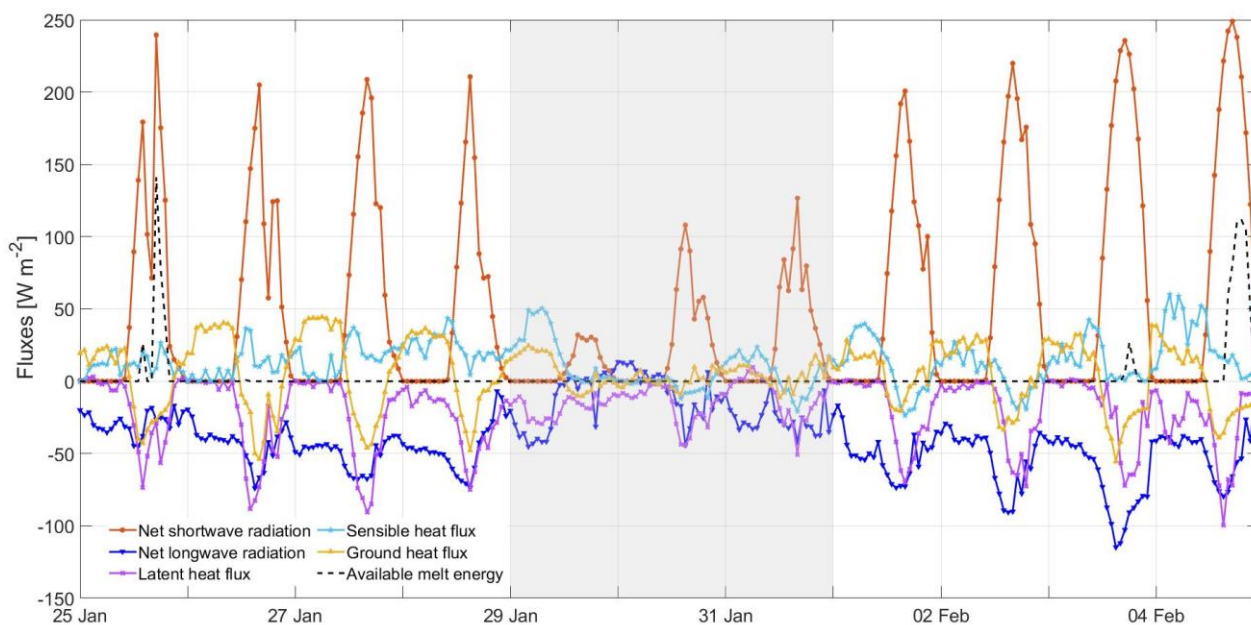
275

Figure 6. Glacier energy balance surface fluxes estimated by COSIPY model forced with the Olivares Alfa AWS (Fig. 1). The grey area corresponds to the dates of the AR event according to Valenzuela et al. (2022).

4.4 Simulation of the Olivares Alfa Glacier mass balance

The simulated mass balance of the Olivares Alfa Glacier for the hydrological years (April-May) between 2014/15 and 2020/21
280   are shown in Figure 7. Five of all 7 years finished with negative mass balance, with the 2019/20 year being the most negative year (-3.2 m w.e.). The 2018/19 year was barely positive, while the 2016/17 finished with a positive mass balance of 0.25 m w.e., with the mean of the 7-years period being -0.8 m w.e. Typically, ablation in April dominates the mass balance, occasionally interrupted by snow accumulation events at different dates depending on the hydrological year. The 2015/16 year shows that the ablation ceased due to temperature drops, not by accumulation, stabilising at around -0.5 m w.e. before the first
285   accumulation event in July. The hydrological year 2016/17 was particular due to a significant accumulation event in April.
The hydrological year 2020/21 shows a period of accumulation concentrated mainly during June (see Fig. 7). Before this month, no important accumulation events were observed at the start of the hydrological year (April-May) dominated by melting. After July, no important accumulation events were observed, keeping the mass balance close to equilibrium. As expected, the ablation season started in September 2020, albeit gradually. No accumulation events were observed in the
290   ablation season until the January 2021 AR event. In spring and part of the summer, the mass balance experienced a gradual

13

decrease, primarily due to melting. This tendency was abruptly interrupted by the January 2021 AR event. Compared to previous years and due to the AR event, the mass balance of this hydrological year was among the least negative within the analysed period, like the 2015/16 and the 2018/19 hydrological years. The spatial distribution of the mass balance is shown in Figure S1. As expected, a spatial gradient in the mass balance is evident, with a consistently larger mass loss in the frontal

295 zone at all the years. The hydrological years 2014/15 and 2019/20 experienced their most significant surface mass loss.

We performed a sensitivity experiment in the mass balance simulation during the 2020/21 hydrological year, assuming the AR event did not occur (Fig. 8). In this hypothetical scenario, the mass balance would have negatively ranged between -2.4 and -0.6 m w.e. (mean of -1.5 m w.e.), instead of the near zero observed, underscoring the significant impact of this singular accumulation event in the ablation season on the annual mass balance.
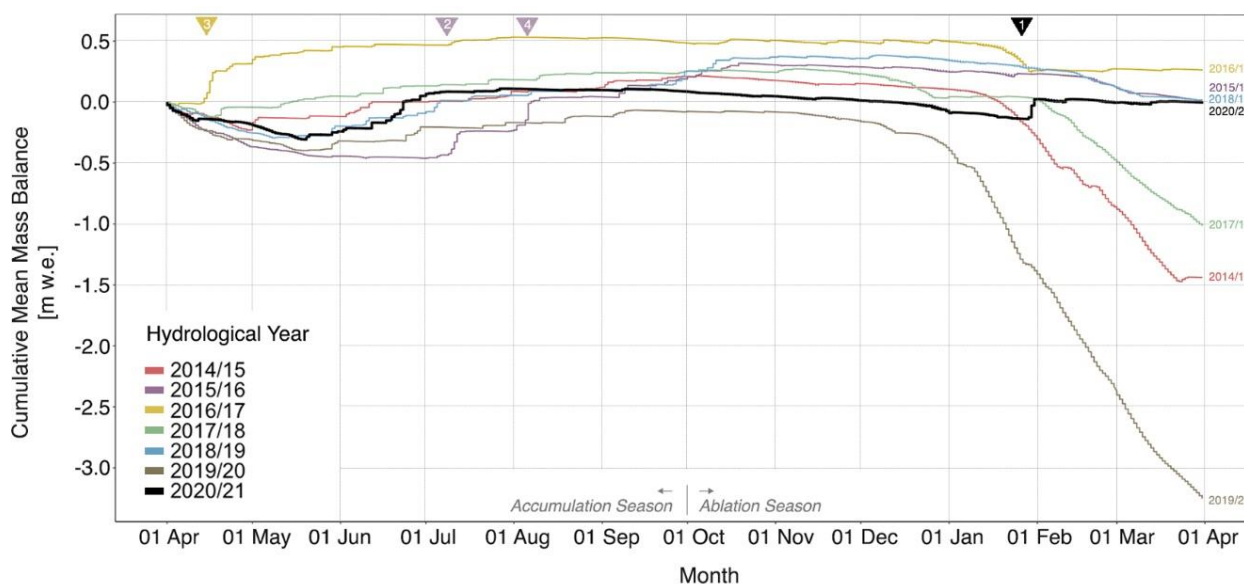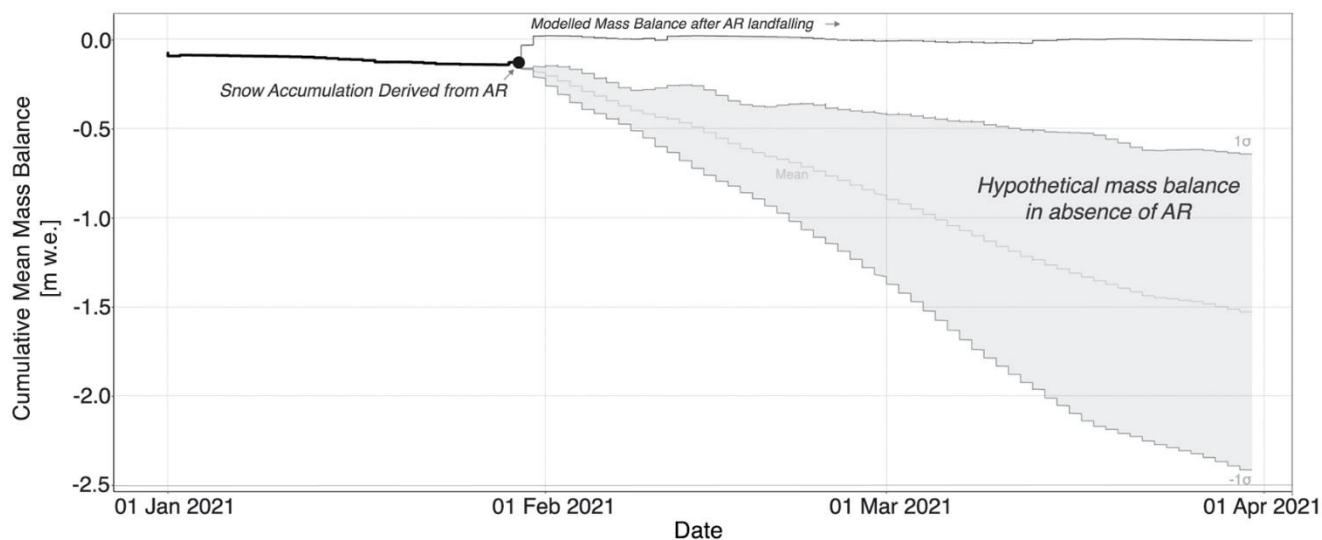
300

Figure 7. Accumulated total mass balance of the Olivares Alfa glacier for seven hydrological years (from 2014/15 to 2020/2021). Triangles at the top are ARs events mentioned in the text with their respective categorization.

305

Figure 8. Glacier mass balance scenarios for the 2020/21 hydrological year without occurrence of the January 2021 AR event. The graph shows a zoom for the period January to March 2021. The uncertainty range corresponds to 1σ.

5 Discussion

5.1 Modelling approach: Uncertainties and comparison with previous studies

310 The modelling approach incorporates several parameterizations and assumptions which may introduce uncertainty to the outputs of the model. For instance, using a constant lapse rate for air temperature. This rate is spatially and temporally dependent on meteorological conditions (e.g., Bravo et al., 2019a). Snow albedo is highly parameterized following the snow age approach (Sauter et al., 2020; Oerlemans and Knap, 1998), while ice albedo is assumed as constant when snowpack thickness is 0 m. In consequence, ice albedo parameterization neglected ice spatial heterogeneity in a glacier where deposition

315 of light-absorbing impurities from different sources has been detected (Barandun et al. 2022), contributing to a darkening trend on the glacier surface (Shaw et al.; 2021). Moreover, small spatial heterogeneity is not captured by the model as the glacier model runs at 100 m grid size. Indeed, the presence of penitentes on the glacier surface—spiky structures of compacted old snow and ice found on central Chilean glaciers (Lliboutry, 1954)—has been noted in the Olivares River sub-basin glaciers. Indeed, a pre-event picture of Paloma Norte Glacier (Fig. S2, see Fig. 1 for location) shows the existence of penitentes. This

320 glacier feature significantly affects energy balance fluxes by altering net shortwave and longwave radiation compared to a flat surface (Corripio and Purves, 2005).

Despite these complexities, the model's primary focus is to evaluate the impact of AR events on the mass balance, not to precisely replicate the exact conditions of the Olivares Alfa Glacier. Thus, the model maintains consistent parameters across each hydrological year to evaluate the general surface energy fluxes and mass balance of the glacier. While no direct

325 measurements of energy balance fluxes for Olivares Alfa Glacier exist, similar modelling and observational analyses have been conducted on nearby glaciers such as the Juncal Norte in the Aconcagua River Basin, as well as on the Bello and the San Francisco in the Maipo River basin (Ayala et al., 2017; Schaefer et al., 2020), all of them focusing on summer months. When comparing summertime mean values for different glaciers (Table 2), a consensus exists that net shortwave radiation and sensible heat fluxes function as sources of energy, whereas net longwave radiation and latent heat fluxes act as energy sinks.

330 **Table 2. Comparison of energy balance fluxes estimated in summertime by this work (Olivares Alfa Glacier) and by previous studies in nearby glaciers of central Chile.**

Glacier	Olivares Alfa	Juncal Norte	Bello	San Francisco
Net shortwave radiation (W m^{-2})	120	70 to 285	223/220/208	137/135/149
Net longwave radiation (W m^{-2})	-53	-75 to -45	-69/-48/-69	-42/-19/-43
Sensible heat flux (W m^{-2})	18	0 to 65	25(32)/6/32	11(41)/6/13
Latent heat flux (W m^{-2})	-39	-70 to -10	-22(-29)/-33/-22	-2(-9)/-5/-1
Energy balance modelling	Distributed	Distributed	Point-Scale	Point-Scale
Elevation (m a.s.l.)	4284-4988	2904-5896	4134	3466
Aspect	NE	N	SE	SE
Period	Summer (DJF, 2014-2021)	Dec. 2008 to Feb. 2009	Jan.-Mar. 2015	Mar. 2016
Source	This work	Ayala et al. (2017)	Schaefer et al. (2020)*	Schaefer et al. (2020)*

*Schaefer et al.(2020) estimated the energy fluxes using three different approaches.

Radiative and turbulent fluxes in Olivares Alfa align with those previous studies (Table 2), despite the inherent differences due to distributed versus point-scale modelling, varying periods, elevation, and aspect. Juncal Norte and Olivares Alfa glaciers
335 share a similar northward aspect, contrasting with the predominantly southeast-facing San Francisco and Bello glaciers. Characteristics of valley topography and shadow cast effect also contribute to flux spatial variations.

Regarding mass balance, geodetic estimations for Olivares Alfa Glacier over the last twenty years are negative, ranging from -0.5 to -1.2 m w.e., with variations depending on the period (Farias-Barahona et al., 2020; Hugonnet et al. 2021). Estimation by Hugonnet et al. (2021) shows that the mean mass loss in Olivares Alfa reached -1.2 m w.e. for the period 2015-2019,
340 slightly higher than our estimates of -0.9 m w.e. for the same period. Our seven-year model average was -0.8 m w.e.,

comparable to the -0.9 m w.e. (2000-2013) and -0.8 m w.e. (2000-2019) estimates by Farias-Barahona et al. (2020) and Hugonnet et al. (2021), respectively.

The nearby glacier Echaurren Norte (0.2 km^2), monitored annually by the Chilean Water Directorate (DGA) and reported to the World Glacier Monitoring Service (WGMS, 2023), showed a negative mass balance with a mean of -1.9 m w.e. during the

345 same period of this study. This difference is likely due to its elevation range (3650-3880 m a.s.l.). Its interannual variability magnitude is 1.1, versus 1.3 m w.e. for Olivares Alfa. Despite slight discrepancies of 0.1 to 0.3 m w.e. compared to geodetic balances, our modelling result is deemed effective in capturing the atmospheric condition responses and interannual variability for Olivares Alfa.

5.2 A glacier accumulation event rather than a glacier melting event

350 Despite the AR event in January 2021 being a warm midlatitude frontal storm (Valenzuela et al. 2022) and some documentation of ARs with glacier melt events in mid-latitude regions (e.g. Little et al., 2019; Kropač et al. 2021, Box et al., 2022), the January 2021 AR event in the central Andes of Chile predominantly caused snow accumulation for the glaciers in the Maipo River basin glaciers (see Fig. S2 example for Paloma Norte Glacier).

Several factors explain this impact. At synoptic-scale, significant moisture transport. Although humidity by itself is not a factor

355 to determine if an event is accumulation or melt, it determines the magnitude of, in this case, the accumulation on the glacier surface and its imprint in the mass balance 2020/21 (Fig. 7). The IVT value during this event (425 kg m^{-1} s^{-1}) was the highest for January-February events compared to previous years (see Table S1), where typically IVT values during AR events oscillate between 295 and 363 kg m^{-1} s^{-1}. Additionally, the duration of the event contributed significantly to the remarkable rate of accumulation over the glaciers in summer compared to previous years. By comparison, AR events in winter can exhibit much

360 higher IVT values, reaching up to 1056 kg m^{-1} s^{-1}, like the AR category 4 event in early August 2015 (Table S1), which is also reflected in the accumulated mass balance (Fig. 7).

A primary factor to determine accumulation is the freezing level. At the Maipo River basin, post-event snowline elevation was below the elevation of the frontal zones of the lower glaciers which according to Ayala et al. (2020) are around 2600-2700 m a.s.l. However, although snow accumulation was predominant we cannot discard that melt and rain occurred in some glaciers

365 during the event, especially on the lower glaciers in the Maipo River basin.

Glaciers in the Olivares River sub-basin are located above 3500-3600 m a.s.l. (Fig. 1), and the freezing level during the precipitation event descended up to 3200 m a.s.l. Precipitation at the beginning of the event occurs with the 0°C isotherm at around 3600-3800 m a.s.l., suggesting positive temperatures at lower glacier sections and probably sleet-type precipitation. However, as a result, the post-event snowline elevation was around 2500 m a.s.l. This indicates snow accumulation began at

370 temperatures above freezing. Such disparity aligns with the variability of the rain-snow temperature threshold noted in other studies (e.g., Jennings et al., 2018). Indeed, differences of about 280 m between the snowline and the 0°C isotherm are observed during storms in the Andes at 30°S (Schauwecker et al., 2022), which can extend up to ~500 m during high-rate precipitation events. The high precipitation rate during the event occurred with the lower 0°C isotherm calculated as 3250 m a.s.l., while

17

the snowline after the event was estimated at 2460 m a.s.l., indicating a 790 m difference. Furthermore, the 2°C isotherm,
375 commonly used to define the rain-snow partitioning (e.g. Koppes et al., 2011; Bravo et al., 2019b), reached a minimum
elevation of 2800 m a.s.l. (Fig. 4), still above the detected snowline.

Over the Olivares Alfa Glacier, snow accumulation is expected on its surface even during summer. Figure 9 shows the hourly
precipitation and its corresponding temperatures recorded in January and February between 2014 and 2021 by the GEONOR
and the AWSOA (Fig. 1). Overall, hourly events larger than 1-2 mm h^{-1} occur with negative temperatures, or up to 2°C,
380 meaning that snow and sleet prevail. Events with temperatures greater than 2°C are less frequent and weak, usually in the 0.1
to 1 mm h^{-1} precipitation rate range. These warm rain events may come from weak high-mountain convective cells, typical of
the summertime in the western slope of the Andes (Viale et al., 2014). However, despite snow accumulation being common
in summer months, the impact of the AR resulted in no available melt energy during and after the event. During summertime,
the availability of melt energy is typical in subtropical Andean glaciers and even at the elevation of Olivares Alfa Glacier
385 (Table 2). Reduction of temperature and humidity gradients between the atmosphere and glacier surface reduces the magnitude
of the turbulent fluxes. Further, cloud cover forces a decrease of net shortwave radiation, while net longwave radiation remains
a net sink, only briefly becoming an energy source (Fig. 6). These conditions cannot be generalised for all the Maipo glaciers,
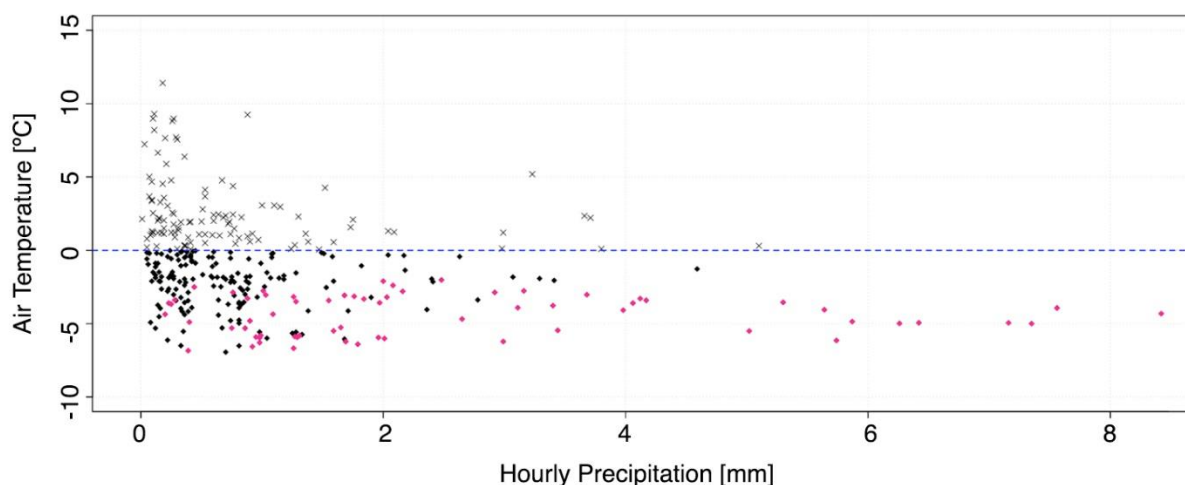though.

390 **Figure 9. Scatter-plot of the precipitation events recorded by the GEONOR and air temperature recorded by AWSOA. Hourly data**
corresponds to January and February for the years 2014 to 2021. Crosses are the precipitation events with positive air temperatures
and diamond with negative air temperatures. Pink diamonds are the precipitation rates during the event at the end of January 2021.

Conversely, Brewster Glacier (44°S, elevation range of 1700-2400 m a.s.l.) in the Southern Alps experienced increased heat
395 turbulent fluxes from the atmosphere to the glacier during a summer AR event (6 February 2011; Kropač et al. 2021),
generating the energy available for melting there. The main environmental differences between Glaciers in the Southern Alps
and those in the subtropical Andes are related to the geographic and climatic conditions. Olivares Alfa is a high-elevation

18

glacier with a relatively dry atmosphere, while Brewster Glacier is located at a lower elevation in a maritime environment. Both glaciers naturally experienced reduced net shortwave radiation during the summertime AR events due to cloud cover.

400 However, while cloud cover, precipitation type and air temperature during the summer AR event contribute to energy source through influx longwave radiation at the Brewster Glacier, they contribute to energy sink at the Olivares Alfa glacier. For the latent heat flux, the AR event's moisture input increased humidity gradient at Brewster Glacier, enhancing latent heat flux, whereas at Olivares Alfa Glacier, the atmosphere's humidity neared surface conditions, reducing the gradient. Sensible heat flux increased at Brewster Glacier due to higher atmospheric temperatures compared to the glacier surface, contrasting the

405 decreased flux at Olivares Alfa, where air temperature approached surface temperatures, reducing the energy available for melting. The conditions at Brewster Glacier during AR events may align closely with those observed in glaciers situated in Patagonian environments (Brown, 2020), highlighting the varied impacts of AR events based on geographic and climatic settings.

5.3 Seasonal conditions vs one extreme event

410 A regional signature of this particular AR event can be determined for all glaciers in the Maipo River basin. The mass balance record of Echaurren Norte Glacier (WGMS, 2023) shows that 2020/21 was the second less negative (-0.7 m w.e.) hydrological year since 2010, only surpassed by the 2016/17 hydrological year (-0.4 m w.e.). It is generally accepted that glacier mass balance in the subtropical Andes is influenced by the interannual variability of the snow accumulation (Masiokas et al., 2016), which is often linked to ENSO conditions, with El Niño conditions typically bringing higher amount of snow accumulation

415 (Cortez and Margulis, 2017). This suggests a correlation between El Niño conditions and positive glacier mass balance, as observed at Echaurren Norte Glacier (Farias-Barahona et al., 2019). Furthermore, AR frequency is anticipated to rise during the El Niño phases (Saavedra et al., 2020; Campos and Rondanelli, 2023). The 2020/21 year, however, was dominated by La Niña, notably during the summer when the AR event occurred, contrary to the usual El Niño conditions as indicated by negative sea-surface temperature anomalies of around -1°C in the ENSO 3.4 region. These conditions and our findings give insights

420 into how an extraordinary and unseasonal snow accumulation event can significantly impact the glacier mass balance, extending beyond the usual impacts of large-scale drivers like ENSO.

As we showed, the mass balance of Olivares Alfa Glacier in 2020/21 was near the equilibrium. Without the AR event, it would have been significantly more negative, potentially rivalling or surpassing the second most negative mass balance recorded in 2014/15. This is likely according to our statistical scenarios (Fig. 8) but also supported by the higher spring snowline elevation

425 over the past 20 years (Fig. 3) and below-average winter-spring precipitation (April to December) as recorded by the Lagunitas meteorological station (-33.08, -70.25, 2765 m a.s.l., Fig. S3) during 1991-2021. However, the 2020/2021 mass balance was comparable to 2015/16 and 2018/19, the two years with the highest winter accumulation rate during the seven years analysed in the Olivares River sub-basin. In particular, the 2015/16 year experienced two major winter AR events under El Niño conditions, one in mid-July and another between August 5 and 9 (category 4).

19

430 The 2016/17 hydrological year had the most positive mass balance, characterized by an important accumulation event in April 2016, which indeed was an atmospheric river category 3 (Fig. 7, Table S1). After several accumulation events of lower magnitude in winter and spring 2016, the mass balance stabilised at about 0.5 m w.e. until ablation started in January 2017. Early in the year, El Niño conditions favoured AR events (Saavedra et al., 2020; Campos and Rondanelli, 2023), but the latter part shifted to neutral and La Niña conditions, leading to the coldest September-December period compared to other years

435 (Fig. S4). These colder conditions delayed ablation's onset at Olivares Alfa Glacier during the 2016/17 hydrological year. Contrary to typical expectations, this year's positive balance was during predominant La Niña conditions, significantly impacted by a single AR event, illustrating how ENSO and AR events jointly influenced the 2016/17 annual mass balance. It is important to remark that the impact is not solely from the event itself. Feedback mechanisms related to snow accumulation also impact the mass balance. After the event, ablation diminished due to reduced surface temperatures and increased albedo,

440 which lowered net shortwave radiation, which is the main source of energy for melting during summer.

6 Conclusions

In this study, we investigated the impact of an unseasonal atmospheric river (AR) and its associated unusual summertime heavy orographic precipitation on the mass balance of the Olivares Alfa Glacier in the Maipo River basin. The Maipo River is the main water source for Santiago, Chile's densely populated capital, supporting its residents, agriculture, and industry. This

445 summer AR transported a large amount of water vapour from lower latitudes, impacting central Chile at the end of January 2021 and producing an extraordinary and unseasonal orographic precipitation event in the subtropical Andes (Valenzuela et al 2022).

By utilizing remote sensing, meteorological in-situ observations, and glacier modelling, we thoroughly assessed the impacts of this AR-driven precipitation event. A lower than normal 0°C isotherm and a snowline below glacier's elevation range were

450 detected during and after the event, indicating predominant snow accumulation across the glaciers of the Olivares River sub-basin, and potentially the entire Maipo River basin's glaciers.

Modelling of the Olivares Alfa Glacier shows that the high unseasonal snow accumulation has a significant role in altering the annual mass balance. This mass glacier accumulation abruptly interrupted the ongoing summertime melting trend for the rest of the ablation season, significantly reducing the ablation rates due to snow-albedo feedback and decreased glacier surface

455 temperatures. Surface energy balance analysis shows that melting energy was absent during the event, mainly due to the reduction of the typical source of energy in summer, i.e., net shortwave radiation and sensible heat flux. Although the energy sinks, such as net longwave radiation and latent heat flux, saw a reduction in their magnitude, they did not offset the decrease in the energy sources.

As a consequence, the 2020/21 annual balance was near equilibrium (∼0 m w.e.), despite the high spring snowline and below-

460 normal winter precipitation typical of La Niña conditions. In the context of seven simulated hydrological years (from 2014/15 to 2020/21), the annual mass balance of the 202/21 year resembled those seen in last El Niño years, underscoring how an extraordinary accumulation event can offset expected responses to large-scale climatic drivers like ENSO.

In a warming climate, ARs are projected to become more frequent (Nellikkattil et al., 2023) and intense in terms of their precipitation rate (Wang et al., 2023). Given the impact on glacier mass balance of unseasonal snow accumulations tied to ARs, like the January 2021 event, we anticipate a growing influence of such events on Andean glaciers, particularly when they occur out of season. Moreover, in addition to causing unseasonal snow accumulations, ARs have the potential to trigger significant melting events. The occurrence of unseasonal extreme precipitation events, whether they lead to accumulation or melting, will introduce new challenges in our way of analysing glacier mass balance data, necessitating enhanced in-situ campaigns, more comprehensive mass balance observations, and expanded modelling efforts to better understand the spatiotemporal variability and impacts of such extreme events on glacier dynamics.

Author contributions

CB, SC and MV designed the outline of this study, PP prepared the weather station data and calculated 0°C isotherm, NGL prepared the ERA5 data, SC run the model and calculated snowline, MV catalogue the historic atmospheric river events. CB, SC, MV and PP contribute with the figures. CB and SC analysed the data and write the manuscript. DB and MV provide guidance on results interpretation. MV, NGL and DB reviewed and edited the paper. All authors contributed to the final paper.

Competing interests

The authors declare that they have no conflict of interest.

Acknowledgments

Funding

References

Adusumilli, S., Fish, M. A., Fricker, H. A., and Medley, B.: Atmospheric river precipitation contributed to rapid increases in

490   surface height of the West Antarctic Ice Sheet in 2019, Geophys. Res. Lett., 48, e2020GL091076, https://doi.org/10.1029/2020GL091076, 2021.

Ayala, A., Pellicciotti, F., Peleg, N., and Burlando, P.: Melt and surface sublimation across a glacier in a dry environment: distributed energy-balance modelling of Juncal Norte Glacier, Chile, J. Glaciol., 63, 803–822, https://doi.org/10.1017/jog.2017.46, 2017.

495 Ayala, Á., Farías-Barahona, D., Huss, M., Pellicciotti, F., McPhee, J., and Farinotti, D.: Glacier runoff variations since 1955 in the Maipo River basin, in the semiarid Andes of central Chile, Cryosphere, 14, 2005–2027, https://doi.org/10.5194/tc-14-2005-2020, 2020.

Barandun, M., Bravo, C., Grobety, B., Jenk, T., Fang, L., Naegeli, K., Rivera, A., Cisternas, S., Münster, T., and Schwikowski, M.: Anthropogenic influence on surface changes at the Olivares Glaciers; Central Chile, Sci. Total. Environ., 833, 155068,

500   https://doi.org/10.1016/j.scitotenv.2022.155068, 2022.

Barcaza, G., Nussbaumer, S., Tapia, G., Valdés, J., García, J., Videla, Y., Albornoz, A., and Arias, V.: Glacier inventory and recent glacier variations in the Andes of Chile, South America, Ann. Glaciol., 58, 1–15, https://doi.org/10.1017/aog.2017.28, 2017.

Box, J. E., Wehrlé, A., van As, D., Fausto, R. S., Kjeldsen, K. K., Dachahuer, A., Ahlstrøm, A. P., and Picard, G.: Greenland

505   Ice Sheet rainfall, heat and albedo feedback impacts from the mid-August 2021 Atmospheric River, Geophys. Res. Lett., 49, e2021GL097356, https://doi.org/10.1029/2021GL097356, 2022.

Bozkurt, D., Rondanelli, R., Garreaud, R., and Arriagada, A.: Impact of warmer eastern tropical Pacific SST on the March 2015 Atacama floods, Mon. Weather. Rev., 144, 4441-4460, https://doi.org/10.1175/MWR-D-16-0041.1, 2016.

Bozkurt, D., Marín, J., and Barrett, B.: Temperature and moisture transport during atmospheric blocking patterns around the

510   Antarctic Peninsula, Weather Clim. Extrem., 38, 100506, https://doi.org/10.1016/j.wace.2022.100506, 2022.

Braun, M.H., Malz, P., Sommer, C., Farias-Barahona, D., Sauter, T., Casassa, G., Soruco, A., Skvarca, P., and Seehaus, T.: Constraining glacier elevation and mass changes in South America, Nat. Clim. Change., 9, 130–136, https://doi.org/10.1038/s41558-018-0375-7, 2019.

Bravo, C., Quincey, D.J., Ross, A.N., Rivera, A., Brock, B., and Silva, A.: Air temperature characteristics, distribution, and

515   impact on modeled ablation for the South Patagonia Icefield, J. Geophys. Res-Atmos., 124, 907–925, https://doi.org/10.1029/2018JD028857, 2019a.

Bravo, C., Bozkurt, D., Gonzalez-Reyes, Á., Quincey, D.J., Ross, A.N., Farías-Barahona, D., and Rojas, M.: Assessing snow accumulation patterns and changes on the Patagonian Icefields, Front. Environ. Sci., 7:30, https://doi.org/10.3389/fenvs.2019.00030, 2019b.

520   Brown, S.S.: The impact of subtropical atmospheric rivers on Patagonian glaciers, M.Sc. thesis, Faculty of Science and Engineering, Macquarie University, 95 pp, https://doi.org/10.25949/20541267.v1, 2020.

Campos, D., and Rondanelli, R.: ENSO-related precipitation variability in Central Chile: The role of large scale moisture transport, J. Geophys. Res-Atmos. 128, e2023JD038671, https://doi.org/10.1029/2023JD038671, 2023.

Carey, M., Huggel, C., Bury, J., Portocarrero, C., and Haeberli, W.: An integrated socio-environmental framework for glacier
525   hazard management and climate change adaptation: lessons from Lake 513, Cordillera Blanca, Perú, Climatic Change, 112, 733–767, https://doi.org/10.1007/s10584-011-0249-8, 2012.

Chen, X., Leung, L.R., Wigmosta, M., and Richmond, M.: Impact of atmospheric rivers on surface hydrological processes in western U.S. watersheds. J. Geophys. Res-Atmos.,124, 8896–8916. https://doi.org10.1029/2019JD030468, 2019.

Crespo, S.A., Lavergne, C., Fernandoy, F., Muñoz, A. A., Cara, L., and Olfos-Vargas, S.: Where does the Chilean Aconcagua
530   river come from? Use of natural tracers for water genesis characterization in glacial and periglacial Environments, Water, 12, 2630. https://doi.org/10.3390/w12092630, 2020.

Corripio, J.G., and Purves, R.S.: Surface energy balance of high-altitude glaciers in the Central Andes: The effect of snow penitentes, in: Climate and Hydrology in Mountain Areas, edited by: de Jong, C., Collins, D., and Ranzi, R., Wiley, London, 15-27, https://doi.org/10.1002/0470858249.ch3, 2005.

535   Cortés, G. and Margulis, S.: Impacts of El Niño and La Niña on interannual snow accumulation in the Andes: Results from a high-resolution 31 year reanalysis, Geophys. Res. Lett., 44, 6859–6867, https://doi.org/10.1002/2017GL073826, 2017.

Demortier, A., Bozkurt, D., and Jacques-Coper, M.: Identifying key driving mechanisms of heat waves in central Chile, Clim. Dynam., 57, 2415–2432, https://doi.org/10.1007/s00382-021-05810-z, 2021.

Dolant, C., Langlois, A., Brucker, L., Royer, A., Roy, A., and Montpetit, B.: Meteorological inventory of rain-on-snow events
540   in the Canadian Arctic Archipelago and satellite detection assessment using passive microwave data. Physical Geography 39(5), 428–444, https://doi.org/10.1080/02723646.2017.1400339, 2017.

Dussaillant, I., Berthier, E., Brun, F., Masiokas, M., Hugonnet, R., Favier, V., Rabatel, A., Pitte, P., and Ruiz, L.: Two decades of glacier mass loss along the Andes, Nat. Geosci., 12, 802–808, https://doi.org/10.1038/s41561-019-0432-5, 2019.

Farías-Barahona, D., Vivero, S., Casassa, G., Schaefer, M., Burger, F., Seehaus, T., Iribarren-Anacona, P., Escobar, F., and
545   Braun, M.H.: Geodetic mass balances and area changes of Echaurren Norte Glacier (Central Andes, Chile) between 1955 and 2015, Remote Sens., 11, 260, https://doi.org/10.3390/rs11030260, 2019.

Farías-Barahona, D., Ayala, Á., Bravo, C., Vivero, S., Seehaus, T., Vijay, S., Schaefer, M., Buglio, F., Casassa, G., Braun, M.H.: 60 Years of Glacier Elevation and Mass Changes in the Maipo River Basin, Central Andes of Chile, Remote Sens., 12, 10, 1658-1658, https://doi.org/10.3390/rs12101658, 2020.

550   Feron, S., Cordero, R., Damiani, A., Llanillo, P.J., Jorquera, J., Sepulveda, E., Asencio, V., Laroze, D., Labbe, F., Carrasco, J., and Torres, G.: Observations and Projections of Heat Waves in South America, Sci. Rep., 9, 8173, https://doi.org/10.1038/s41598-019-44614-4, 2019.

Garreaud, R., Vuille, M., Compagnucci, R., and Marengo, J.: Present-day South American climate, Palaeogeogr. Palaeocl., 281, 180-195, https://doi.org/10.1016/j.palaeo.2007.10.032, 2009.

555   Garreaud, R. D., Boisier, J. P., Rondanelli, R., Montecinos, A., Sepúlveda, H. H., and Veloso-Aguila, D.: The Central Chile Mega Drought (2010–2018): A climate dynamics perspective, Int. J. Climatol., 40, 421–439, https://doi.org/10.1002/joc.6219, 2019.

Garreaud, R., Jacques-Coper, M., Marín, J.C., Narváez, D.A.: Atmospheric rivers in South-Central Chile: Zonal and tilted events. Atmosphere, 15, 406, https://doi.org/10.3390/atmos15040406, 2024.

560   González-Reyes, Á., Jacques-Coper, M., Bravo, C., Rojas, M., and Garreaud, R.: Evolution of heatwaves in Chile since 1980, Weather Clim. Extrem., 41, 100588, https://doi.org/10.1016/j.wace.2023.100588, 2023.

Guan, B., Molotch, N.P., Waliser, D.E., Fetzer, E.J., and Neiman, P.J.: Extreme snowfall events linked to atmospheric rivers and surface air temperature via satellite measurements, Geophys. Res. Lett., 37, L20401. https://doi.org/10.1029/2010GL044696, 2010.

565   Guan, B., Waliser, D.E., Ralph, F.M., Fetzer, E.J. and Neiman, P.J.: Hydrometeorological characteristics of rain-on-snow events associated with atmospheric rivers, Geophys. Res. Lett., 43, 2964–2973, https://doi.org/10.1002/2016GL067978, 2016.

Guan, B., and Waliser, D.E.: Tracking atmospheric rivers globally: Spatial distributions and temporal evolution of life cycle characteristics, J. Geophys. Res-Atmos., 124, 12523–12552, https://doi.org/10.1029/2019JD031205, 2019.

570   Hall, D. K., Riggs, G. A., and Salomonson, V. V.: MODIS snow and sea ice products, in: Earth Science Satellite Remote Sensing, Springer, 154–181, https://doi.org/10.1007/978-3-540-37293-6_9, 2006.

Hersbach, H., Bell, B., Berrisford, P., Hirahara, S., Horányi, A., Muñoz-Sabater, J., Nicolas, J., Peubey, C., Radu, R., Schepers, D., Simmons,A., Soci, C., Abdalla, S., Abellan, X., Balsamo, G., Bechtold, P., Biavati, G., Bidlot, J., Bonavita, M., De Chiara, G., Dahlgren, P., Dee,D., Diamantakis, M., Dragani, R., Flemming, J., Forbes, R., Fuentes, M., Geer, A., Haimberger,

575   L., Healy, S., Hogan, R. J., Hólm, E.,Janisková, M., Keeley, S., Laloyaux, P., Lopez, P., Lupu, C., Radnoti, G., de Rosnay, P., Rozum, I., Vamborg, F., Villaume, S., and Thépaut,J.-N.: The ERA5 global reanalysis, Q. J. Roy. Meteor. Soc., 146, 19992049, https://doi.org/10.1002/qj.3803, 2020.

Hugonnet, R., McNabb, R., Berthier, E. Menounos, B., Nuth, C., Girod, L., Farinotti, D., Huss, M., Dussaillant, I., Brun, F., and Kääb, A.: Accelerated global glacier mass loss in the early twenty-first century, Nature, 592, 726–73,
580   https://doi.org/10.1038/s41586-021-03436-z, 2021.

Jacques-Coper, M., Brönnimann, S., Martius, O., Vera, C., and Cerne, B.: Summer heat waves in southeastern Patagonia: an analysis of the intraseasonal timescale, Int. J. Climatol., 36, 1359– 1374, https://doi.org/10.1002/joc.4430, 2016.

Jacques-Coper, M., Veloso-Águilam D., Segura, C., and Valencia, A.: Intraseasonal teleconnections leading to heat waves in central Chile. Int. J. Climatol., 41, 4712-4731, https://doi.org/10.1002/joc.7096, 2021.

585   Jennings, K.S., Winchell, T.S., Livneh, B., and Molotch, N.: Spatial variation of the rain–snow temperature threshold across the Northern Hemisphere, Nat. Commun., 9, 1148, https://doi.org/10.1038/s41467-018-03629-7, 2018.

Koppes, M., Conway, H., Rasmussen, L. A., and Chernos, M.: Deriving mass balance variations and calving variations from reanalysis data and sparse observations, Glaciar San Rafael, northern Patagonia, 1950-2005, The Cryosphere 5, 791–808, https://doi.org/10.5194/tc-5-791-2011, 2011.

590 Krajčí, P., Holko, L., Perdigão, R.A.P., Parajka, J.: Estimation of regional snowline elevation (RSLE) from MODIS images for seasonally snow covered mountain basins, J. Hydrol., 519, 1769–1778, https://doi.org/10.1016/j.jhydrol.2014.08.064, 2014.

Kropač, E., Mölg, T., Cullen, N.J., Collier, E., Pickler, C., and Turton, J.V.: A detailed, multi-scale assessment of an atmospheric river event and its impact on extreme glacier melt in the Southern Alps of New Zealand, J. Geophys. Res-

595 Atmos.,126, e2020JD034217, https://doi.org/10.1029/2020JD034217, 2021.

Leung, L.R., and Qian, Y.: Atmospheric rivers induced heavy precipitation and flooding in the western US simulated by the WRF regional climate model, Geophys. Res. Lett., 36, L03820. https://doi.org/10.1029/2008GL036445, 2009.

Lliboutry, L.: The origin of penitents. J. Glaciol., 2, 331–338, https://doi.org/10.3189/S0022143000025181, 1954.

Little, K., Kingston, D.G., Cullen, N.J. and Gibson, P.B.: The role of atmospheric Rivers for extreme ablation and snowfall

600 events in the Southern Alps of New Zealand, Geophys. Res. Lett., 46, 2761-2771, https://doi.org/10.1029/2018GL081669, 2019.

Lopes, F.M., Dutra, E., and Trigo, I.F.: Integrating reanalysis and satellite cloud information to estimate surface downward long-wave radiation, Remote. Sens, 14, 1704, https://doi.org/10.3390/rs14071704, 2022.

Maclennan, M.L., Lenaerts, J.T., Shields, C., and Wille, J.D.: Contribution of atmospheric rivers to Antarctic precipitation,

605 Geophys. Res. Lett., 49, e2022GL100585, https://doi.org/10.1029/2022GL100585, 2022.

Malmros, J. K., Mernild, S. H., Wilson, R., Yde, J. C., and Fensholt, R.: Glacier area changes in the central Chilean and Argentinean Andes 1955–2013/14, J. Glaciol., 62, 391–401, https://doi.org/10.1017/jog.2016.43, 2016.

Masiokas, M. H., Christie, D. A., Le Quesne, C., Pitte, P., Ruiz, L., Villalba, R., Luckman, B. H., Berthier, E., Nussbaumer, S. U., Gonzälez-Reyes, Á., McPhee, J., and Barcaza, G.: Reconstructing the annual mass balance of the Echaurren Norte

610 glacier (Central Andes, 33.5°S) using local and regional hydroclimatic data, The Cryosphere, 10, 927–940, https://doi.org/10.5194/tc10-927-2016, 2016.

Masiokas, M. H., Rabatel, A., Rivera, A., Ruiz, L., Pitte, P., Ceballos, J. L., Barcaza, G., Soruco, A., Bown, F., Berthier, E., Dussaillant, I., and MacDonell, S.: A Review of the current state and recent changes of the Andean cryosphere, Front. Earth Sci., 8, 99, https://doi.org/10.3389/feart.2020.00099, 2020.

615 Mattingly, K.S., Motem T.L., and Fettweis, X.: Atmospheric river impacts on Greenland Ice Sheet surface mass balance, J. Geophys. Res-Atmos., 123, 8538–8560, https://doi.org/10.1029/2018JD028714, 2018.

Mattingly, K.S., Turton, J.V., Wille, J.D., Noël, B., Fettweis, X., Rennermalm, A.K., and Mote, T.: Increasing extreme melt in northeast Greenland linked to foehn winds and atmospheric rivers, Nat. Commu., 14, 1743, https://doi.org/10.1038/s41467-023-37434-8, 2023.

620   Neiman, P.J., Schick, L.J., Ralph, F.M., Hughes, M., and Wick, G.A.: Flooding in western Washington: The connection to atmospheric rivers, J. Hydrometerol., 12, 1337–1358. https://doi.org/10.1175/2011JHM1358.1, 2011.

Nellikkattil, A.B., Lee, J.Y., Guan, B., Timmermann, A., Lee, S.S., Chu, J.E. and Lemmon, D.: Increased amplitude of atmospheric rivers and associated extreme precipitation in ultra-high-resolution greenhouse warming simulations, Commun. Earth Environ., 4, 313, https://doi.org/10.1038/s43247-023-00963-7, 2023.

625   Oerlemans, J. and Knap, W.H.: A one-year record of global radiation and albedo from the ablation zone of the Morteratschgletscher, Switzerland, J. Glaciol., 44, 231–238, https://doi.org/10.3189/S0022143000002574, 1998.

Payne, A.E., Demory, M., Leung, L.R., Ramos, A.M., Shields, C.A., Rutz, J.J. and Ralph, F.M.: Responses and impacts of atmospheric rivers to climate change, Nat. Rev. Earth Environ., 1, 143–157. https://doi.org/10.1038/s43017-020-0030-5, 2020.

630   Poveda, G., Espinoza, J.C., Zuluaga, M.D., Solman, S.A., Garreaud, R., and van Oevelen, P.J.: High Impact Weather Events in the Andes, Front. Earth Sci., 8, 162, https://doi.org/10.3389/feart.2020.00162, 2020.

Ralph, F.M., Neiman, P.J., Wick, G.A., Gutman, S.I., Dettinger, M.D., Cayan, D.R., and White, A.B.: Flooding on California's Russian river: Role of atmospheric rivers, Geophys. Res. Lett., 33, L13801, https://doi.org/10.1029/2006GL026689, 2006.

Ralph, F. M., Rutz, J. J., Cordeira, J. M., Dettinger, M., Anderson, M., Reynolds, D., Schick, L. I., and Smallcomb, C.: A scale
635   to characterize the strength and impacts of atmospheric rivers, B. Am. Meteorol. Soc., 100, 269–290, https://doi.org/10.1175/Bams-D-18-0023.1, 2019.

Rutllant, J.A., Matus, F., Rudloff, V., and Rondanelli, R.: The role of atmospheric rivers in rainfall-induced landslides: A study from the Elqui valley, J. Arid Environ., 216, 105016, https://doi.org/10.1016/j.jaridenv.2023.105016, 2023.

Saavedra, F., Cortés, G., Viale, M., Margulis, S., and McPhee, J.: Atmospheric rivers contribution to the snow accumulation
640   over the Southern Andes (26.5° S–37.5° S), Front. Earth Sci., 8, 1–11, https://doi.org/10.3389/feart.2020.00261, 2020.

Schaefer, M., Fonseca-Gallardo, D., Farías-Barahona, D., and Casassa, G.: Surface energy fluxes on Chilean glaciers: measurements and models, The Cryosphere, 14, 2545–2565, https://doi.org/10.5194/tc-14-2545-2020, 2020.

Sauter, T., Arndt, A., and Schneider, C.: COSIPY v1.3 – an open-source coupled snowpack and ice surface energy and mass balance model, Geosci. Model Dev., 13, 5645–5662, https://doi.org/10.5194/gmd-13-5645-2020, 2020.

645   Schauwecker, S., Palma, G., MacDonell, S., Ayala, Á., and Viale, M.: The Snowline and 0°C Isotherm Altitudes During Precipitation Events in the Dry Subtropical Chilean Andes as Seen by Citizen Science, Surface Stations, and ERA5 Reanalysis Data, Front. Earth Sci., 10, 1–19, https://doi.org/10.3389/feart.2022.875795, 2022.

Shaw, T. E., Ulloa, G., Farías-Barahona, D., Fernandez, R., Lattus, J. M., and McPhee, J.: Glacier albedo reduction and drought effects in the extratropical Andes, 1986–2020, J. Glaciol., 67, 158169, https://doi.org/10.1017/jog.2020.102, 2021.

650   Somos-Valenzuela, M.A., Oyarzún-Ulloa, J.E., Fustos-Toribio, I.J., Garrido-Urzua, N., and Chen, N.: The mudflow disaster at Villa Santa Lucía in Chilean Patagonia: understandings and insights derived from numerical simulation and postevent field surveys, Nat. Hazards Earth Syst. Sci., 20, 2319–2333, https://doi.org/10.5194/nhess-20-2319-2020, 2020.

Valenzuela, R., Garreaud, R., Vergara, I., Campos, D., Viale, M., and Rondanelli, R.: An extraordinary dry season precipitation event in the subtropical Andes: Drivers, impacts and predictability, Weather Clim. Extrem., 37, 100472. https://doi.org/10.1016/j.wace.2022.100472, 2022.

Viale, M., and Garreaud, R.D.: Summer precipitation events over the western slopes of the subtropical Andes, Mon. Weather Rev., 142, 1074–1092, https://doi.org/10.1175/MWR-D-13-00259.1, 2014.

Viale, M., Valenzuela, R., Garreaud, R., and Ralph, F.: Impacts of atmospheric rivers on precipitation in Southern South America, J. Hydrometeorol., 19, 1671–1687, https://doi.org/10.1175/JHM-D-18-0006.1, 2018.

Wang, S., Ma, X., Zhou, S., Wu, L., Wang, H., Tang, Z., Xu, G., Jing, Z., Chen, Z., and Gan, B.: Extreme atmospheric rivers in a warming climate. Nat. Commun., 14, 3219, https://doi.org/10.1038/s41467-023-38980-x, 2023.

WGMS: Global Glacier Change Bulletin No. 5 (2020–2021), edited by: Zemp, M., Gärtner-Roer, I., Nussbaumer, S.U., Welty, E.Z., Dussaillant, I., and Bannwart, J., ISC(WDS)/IUGG(IACS)/UNEP/UNESCO/WMO, World Glacier Monitoring Service, Zurich, Switzerland, 134 pp., publication based on database version: https://doi.org/10.5904/wgms-fog-2023-09, 2023.

Wille, J.D., Favier, V., Dufour, A., Gorodetskaya, I.V., Turner, J., Agosta, C., and Codron, F.; West Antarctic surface melt triggered by atmospheric rivers, Nat. Geosci, 12, 911–916, https://doi.org/10.1038/s41561-019-0460-1, 2019.

Wille, J.D., Favier, V., Gorodetskaya, I.V., Agosta, C., Kittel, C., Beeman, J.C., Jourdain, N.C., Lenaerts, J.T.M., and Codron, F.: Antarctic atmospheric river climatology and precipitation impacts, J. Geophys. Res-Atmos., 126, https://doi.org/10.1029/2020JD033788, 2021.

Wille, J.D., Favier, V., Jourdain, N.C., Kittel, C., Turton, J.V., Agosta, C., Gorodetskaya, I.V., Picard, G., Codron, F., Santos, C.L.D., Amory, C., Fettweis, X., Blanchet, J., Jomelli, V., and Berchet, A.: Intense atmospheric rivers can weaken ice shelf stability at the Antarctic Peninsula, Commun. Earth Environ., 3, 90, https://doi.org/10.1038/s43247-022-00422-9, 2022.

Xu, M., Yu, L., Liang, K., Vihma, T., Bozkurt, D., Hu, X., and Yang, Q.: Dominant role of vertical air flows in the unprecedented warming on the Antarctic Peninsula in February 2020, Commun. Earth Environ., 2, 133, https://doi.org/10.1038/s43247-021-00203-w, 2021.

Zou, X., Bromwich, D.H., Montenegro, A., Wang, S.H., Bai, L.: Major surface melting over the Ross Ice Shelf Part II: Surface energy balance, Q. J. Roy. Meteor. Soc., 147, 2895-2916, https://doi.org/10.1002/qj.4105, 2021.